# Dynamic Reaction inside Co-Rotating Twin Screw Extruder. I. Truck Tire Model Material/Polypropylene Blends

**Sung Hyo Lee, Maridass Balasubramanian, Jin Kuk Kim**

*Department of Polymer Science and Engineering, Division of Advanced Materials, Gyeongsang National University, 900 Jinju, Gyeongnam 660-701, Korea*

Received 12 July 2006; accepted 21 December 2006
DOI 10.1002/app.26489
Published online 15 August 2007 in Wiley InterScience (www.interscience.wiley.com).

**ABSTRACT:** Waste ground rubber tire (WGRT) is a complex composite containing various elastomers, carbon black, zinc oxide, stearic acid, processing oils, and other curatives. Most of the waste ground rubber tire is composed of mainly natural rubber (NR) and styrene butadiene rubber (SBR) in varying proportions. Blending it with other thermoplastic materials is difficult due to the inherent thermodynamic incompatibility. But, the compatibility can be increased by making the reactive sites in WGRT with suitable chemicals under optimum condition of shearing inside a twin screw extruder and it is said to undergo a dynamic reaction inside the extruder. To understand the mechanism of dynamic reaction process of a rubber/polyolefin blend, the blending of a truck tire model material rubber with polyolefin was first tried before it was applied to waste WGRT material. It was observed that the blends of a truck tire model rubber material and PP thermoplastic are physical mixture of two incompatible polymers in which a continuous plastic phase is largely responsible for the tensile properties. The rubber particles are the dispersed phase. The large particle size and the poor adhesion of these rubber particles are believed to be liable for the poor tensile properties. In case of blends of truck tire model material with isotactic polypropylene the tensile properties are found to be lower than that of its PP-*g*-MA counterpart which can be attributed to the reaction of the MA with the carbon black particles. A schematic representation of the possible interactions has been proposed. The effect of addition of compatibilizers such as SEBS and SEBS-*g*-MA has also been studied. The tensile and TGA studies indicate that the polarity of SEBS and SEBS-*g*-MA induces an increase in the performance characteristics for both types of polyolefins but the intensity of this increase is higher in the PP-*g*-MA based blends. © 2007 Wiley Periodicals, Inc. J Appl Polym Sci 106: 3193–3208, 2007

**Key words:** waste ground rubber tire; twin screw extruder; dynamic reaction; truck tire model material

## INTRODUCTION

The importance of recycling the crosslinked rubber used in automotive tires, sealing, and hoses has been well-known.[1–5] Unlike plastics, these thermoset rubbers are difficult to be recycled. The waste ground rubber powders, natural rubber (NR), styrene-butadiene rubber (SBR), and ethylene-propylene-diene rubber (EPDM), obtained by mechanical shredding and grinding of the used rubbers into fragmented particles in a wide range of particle size, have found only limited uses in low performance applications such as the floor materials for playground, tennis and basketball courts, cement modifiers etc. This is attributed to their inferior mechanical properties.

Conventional thermoplastic vulcanizates (TPVs), which are made from virgin rubbers and thermoplastics via dynamic vulcanization using curing agents like sulfur, contain crosslinked rubber particles. The crosslinked rubber phase formed during mixing has a length scale of micrometers and is firmly embedded in the thermoplastic phase, leading to superior mechanical properties.[6]

Of the commercially available thermoplastic elastomers some are expensive, special-purpose materials. The olefin types, which include blends of natural rubber with crystalline polyolefins and those of ethylene propylene terpolymer (EPDM) with polyolefins, are cheaper, and similar in price to the styrene-butadiene-styrene (SBS) block copolymer types of thermoplastic rubbers. The olefinic types have potential uses in flexible automotive components such as bumpers, spoilers requiring materials in the range 90 shore A to 60 shore D.[7,8]

Several works have been reported regarding the processing, vulcanization, and applications of thermoplastic natural rubber.[9] In the present study, a model material based on the recipe of a truck tire involving styrene butadiene rubber (SBR), natural rubber (NR), and butadiene rubber (BR) with other ingredients was blended with isotactic PP and later compared for the effect of dynamic reaction with

*Correspondence to:* J. K. Kim (rubber@gnu.ac.kr).
Contract grant sponsor: Resource Recycling R&D Center.

Journal of Applied Polymer Science, Vol. 106, 3193–3208 (2007)

maleic anhydride grafted polypropylene PP-*g*-MA, SEBS, and SEBS-*g*-MA. In these studies, a constant weight percentage (35 phr) of PP-*g*-MA has been used. as against the same amount of isotactic polypropylene (iPP), relative to 100 phr weight percentage of the truck tire model material. Chemical interactions between the model material and polypropylene matrix has been characterized with Fourier Transform Infra-Red Attenuated Total Reflectance Spectroscopy (FTIR-ATR) and morphological study of fracture surface using SEM. The influence of compatibilizers on the properties of the model material/PP composite has also been investigated. The properties of the blends having SEBS and SEBS-*g*-MA as compatibilizers were compared with both isotactic PP and and maleic anhydride grafted PP (PP-*g*-MA) blends. To understand the mechanism of dynamic reaction process of rubber/polyolefin and the effect of compatibilizer on these compounds, blending of the model material with polyproyplene was first tried and later followed by GRT/PP blends.

## EXPERIMENTAL

### Preparation of model material

The carbon black (CB) filled truck tire model material was mixed using water-cooled Banbury mixer (Dongsin Machinery Corp., BS-B1.6S). The model material recipe is shown in Table I. To improve the mixing quality and to prevent pre-vulcanization, a two-stage mixing process was applied. Firstly, the rubber was premixed in a Banbury mixer at 85°C for 3 min. The rotor speed was 65 rpm and a fill factor of 0.8 was used. After premixing, zinc oxide, stearic acid and paraffin wax were then added and mixed for 1 min. Finally, carbon black (N339) was added to the mixer and the mixing was continued for 2.5 minutes. After the first stage mixing, a two-roll mill of 8-inch (20.32 mm) diameter (Daewoong Machinery Corp.) was used at 50°C in the second stage to prevent any scorch problem during the mixing step.

**TABLE I**
**The Recipe of Model Material**

| Materials | Phr |
|---|---|
| SMR#20 | 16 |
| SBR1502 | 54 |
| BR01 | 30 |
| N339 | 68 |
| A#2 | 18 |
| Other additives | 13 |
| Sulfur | 1.8 |
| CZ | 1.0 |
| DM | 0.5 |
| D | 0.2 |

**TABLE II**
**Model Material/PP Recipe**

| | $VNR_1$ | $VNR_2$ | $VNR_3$ | $VNR_4$ | $VNR_5$ | $VNR_6$ |
|---|---|---|---|---|---|---|
| Model material | 65 | 65 | 65 | 65 | 65 | 65 |
| Isotactic PP | 35 | 35 | 35 | – | – | – |
| PP-*g*-MA | – | – | – | 35 | 35 | 35 |
| SEBS | – | 10 | – | – | 10 | – |
| SEBS-*g*-MA | – | – | 10 | – | – | 10 |

### Materials

The basic materials used in this study and their sources are as follows. PP-*g*-MA (RE 340B, SK Corporation, Korea) is PP functionalized with 0.15 wt % maleic anhydride onto the hydrocarbon chains of polypropylene main chain and isotactic PP (1088, Korea petrochemical, Korea) was purchased locally. The triblock copolymers, SEBS and SEBS-*g*-MA, were supplied by Shell Chemical Co. Ltd., USA. This copolymer has styrene end blocks and hydrogenated butadiene mid block reassembling an ethylene/butylene copolymer. Kraton G1652 containing about 30% wt styrene and molecular weight 79,000 g/mol was used throughout the study. SEBS-*g*-MA(Kraton FG1901X) is SEBS functionalized with 1.84 wt % maleic anhydride onto the hydrocarbon chains of the mid block. Its molecular weight and styrene contents are similar to those of Kraton G1652. The model material/PP blend formulations is shown in Table II.

### Compounding

The most common method for compounding rubber with olefin resins involves the use of intermeshing co-rotating twin screw extruder. Extrusion experiments were carried out on a modular intermeshing twin screw extruder (BauTech BA-19, Korea), a self-wiping corotating extruder with Table III shows the screw characteristics. The screw profile is illustrated in Table IV. Optimum screw configurations, as shown in Figure 1 and Table V was used. The screw speed was maintained at 100 rpm and temperatures profile of the extruder from feeding to the die was 60°C/190°C/220°C/220°C/235°C/235°C/220°C/200°C for PP blends. The extrudate was cooled in a water bath, granulated, and stored.

**TABLE III**
**Technical Data of the Twin Screw Extruder Used**

| Parameter | Value |
|---|---|
| Process length | 40 L/D |
| Barrel diameter | 19.6 mm |
| Screw diameter | 19 mm |
| Helix angle of conveying elements | 17° |
| Radial screw flight clearance | 0.6 mm |
| Channel width of conveying elements | 8.3 mm |
| Flight land width of conveying elements | 20.63 mm |

**TABLE IV**
**Modular Screw Assemblies Used for All Blending experiments**

| Designation | Right-handed screw elements | Left-handed screw elements | Right-handed kneading discs | Neutral kneading discs |
|---|---|---|---|---|
| Screw configuration | 30 (570 mm) | 2 (38 mm) | 26 (123.5 mm) | 3 (28.5 mm) |

Values represent numbers and values in parantheses represent length.

### Preparation of the specimens for tensile testing

The extruders were palletized and then injection molded. The test specimens pertained to ASTM standards[dumbbell shaped samples for tensile strength and elongation at break test (ASTM D412)]. The temperature of the injection molding cylinder was kept at 235°C and the mold temperature was 30 ~ 35°C with the injection pressure at 2000 ~ 24,000 psi.

### Characterizations

#### Fourier transform infrared (FT-IR) spectroscopy

Samples were subjected to IR characterization in the range of 4000–400 $cm^{-1}$ using a Perkin-Elmer 2000 spectrophotometer. The spectra were obtained at a resolution of 4.0 $cm^{-1}$ in the transmission mode. FT-IR spectra of model material/PP composites were taken in the range of 4000–650 $cm^{-1}$ in the attenuated total reflectance mode (FTIR-ATR) using a zinc selenide crystal.

#### Thermogravimetric analysis

For determining the approximate composition of the TPV, thermogravimetric analysis (TGA) was carried out in a DuPont TA2100 thermo gravimetric analyzer in the temperature range of 50–700°C at a heating rate of 20°C/min. The degradation temperature as well as % of loss of mass were calculated from the histograms.

#### Stress–strain properties

Tensile testing was done on dumbbell samples using the UTM (LLOYD INSTRUMENTS, LR10K, UK) as per ASTM D412 at a crosshead speed of 50 mm/min. The test was done at room temperature. The tensile strength (MPa), elongation at break (%) and modulus at 100% and 300% were recorded automatically from the stress-strain plots. For each tensile strength reported, at least five sample measurements were averaged.

#### Dynamic mechanical analysis

The dynamic mechanical properties of blends were studied using a Dynamic Mechanical Analyzer 983 (TA INSTRUMENTS, USA) in the tension mode using rectangular samples (0.5 × 5 × 20 $mm^3$). The test was done in a temperature range of −100°C to 100°C (cooling done with the aid of liquid nitrogen) at a heating rate of 5°C at a frequency of 1 Hz and strain 0.036%. Data were analyzed using TA Instruments Universal Analysis 2000 software, version 3.5B to obtain plots of the loss tangent (tan δ) against temperature.

#### Morphological studies

The phase morphology of the blends was studied by a scanning electron microscopy (FE-SEM, model Philips XL 30S, Netherland) and AFM (Nanoscope IV, Veeco Instruments, Inc., USA). The prepared blend was fractured in liquid nitrogen. Because of a low contrast between the two phases, etching technique was applied in order to extract PP phase at the fracture surface. Xylene was used as the solvent for extraction at 130°C for 30 min and the surface was coated with gold using JFC-1100E ion sputtering device. To study the morphology of the blends using the AFM, the crosssections were microtomed perpendicular to the surface of the plaques and observed directly. The AFM images were obtained in air with a commercial scanning probe microscope. Nanoscope, operating in the tapping mode. Measurements were performed at ambient conditions using rectangular type Si probes with a spring constant of 50 $nm^{-1}$ and resonance frequencies in the 284–364 kHz range. The tip radius was 10 nm. The AFM topographic (height) and elastic (phase) images were simultaneously obtained under normal and hard tapping conditions on the microtomed surface of blends.

### Definition of dynamic reaction mechanism in a twin screw extruder

Polymer blending involves the mixing of a two-phase melt-melt polymeric system. The deformation applied on such systems from the mixer induces an

**Figure 1** Screw configuration used for the model material/PP resins blending experiments.

**TABLE V**
**Geometry and Dimension Data of the Kneading Block**

| Items | First kneading block set | | Second kneading block set | | Third kneading block set | |
|---|---|---|---|---|---|---|
| | L | S | L | S | L | S |
| Number of kneading disc | 5 | 5 | 3 | 4 | – | 7 |
| Paddle orientation | 30° | 30° | 90° | 30° | – | 30° |

L: 9.55 mm Kneading disc, S: 4.75 mm Kneading disc.

increase in interfacial area that is counteracted by interfacial tension. With further deformation of the dispersed phase, a point is reached at which interfacial forces becomes comparable to the deformation rates applied by the blending device. In this stage, interfacial area-reducing processes sets in and the droplets oppose against deformation. Finally, an equilibrium structure, consisting of droplets small enough to resist the disruptive forces will be produced. It is an oversimplification to assume that droplets retain their individuality over the course of the blending process, given that collision of droplets can lead to coalescence, and the resulting morphology is controlled by the balance of breakup and coalescence events.[10]

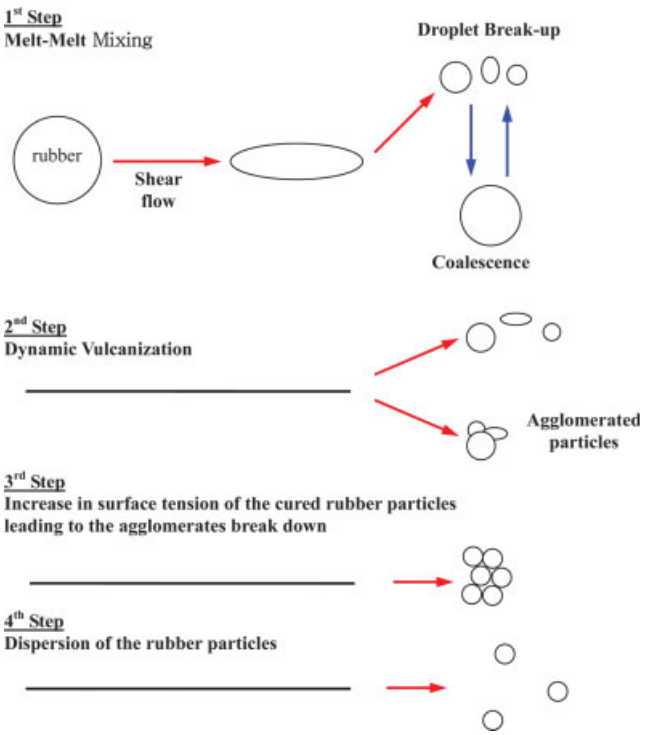


**Figure 2** Schematic diagram of the model describing the mechanism of dynamically cured TPE. [Color figure can be viewed in the online issue, which is available at www.interscience.wiley.com.]

At this juncture, we should not confuse a dynamic reaction with the dynamic vulcanization process which involves the usage of a curing agent/high shear on a thermoplastic-elastomer blend to give a thermoplastic vulcanizate (TPV). Dynamically vulcanized thermoplastic elastomer (TPE) blends were first presented by Fisher[11] and since then have been widely used in the rubber and plastic industries.[12] These materials can be melt-processed and shaped by conventional thermoplastic processing methods but, in their final state, show an elastic recovery similar to that of ordinary vulcanized rubbers.[13] The addition of a small quantity of a vulcanizing system during the melt-mixing of rubber and plastic leads to the *in situ* vulcanization of the dispersed rubber particles as shown in Figure 2. The outstanding properties of these materials are mainly attributed to their specific microstructure, which consists of a continuous plastic matrix with tiny rubber particles dispersed throughout the matrix. This enables the blend to be melt-processed even though the rubber particles are crosslinked. Both the physical and rheological properties of these materials are, therefore, dependent on their morphology. Many works have been done that deals with the mechanical and rheological properties of dynamically cured TPEs. Also, a

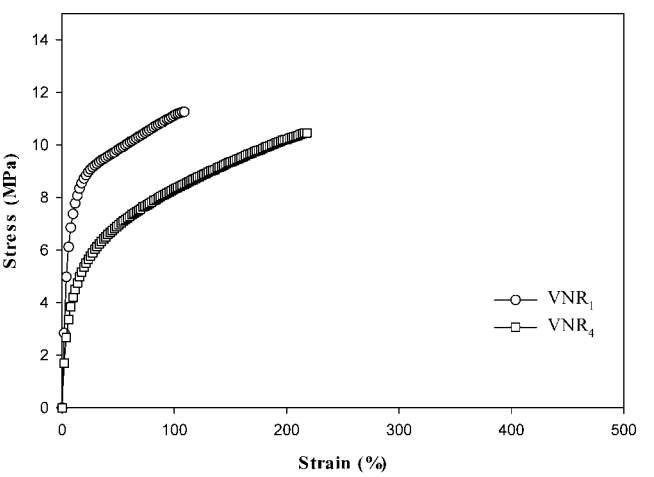


**Figure 3** The tensile properties of model material with isotactic PP and maleic anhydride grafted PP blends.

**TABLE VI**
**Tensile Properties of Model Material/PP Blends**

| | Tensile strength (MPa) | Elongation at break (%) | Modulus (Mpa) | |
|---|---|---|---|---|
| | | | 100% | 300% |
| $VNR_1$ | 11.2 | 109 | 11.1 | – |
| $VNR_2$ | 10 | 150 | 9.2 | – |
| $VNR_3$ | 10.6 | 180 | 9.2 | – |
| $VNR_4$ | 10.5 | 219 | 8.3 | – |
| $VNR_5$ | 10.4 | 359 | 6.9 | 9.8 |
| $VNR_6$ | 11.3 | 430 | 6.6 | 9.8 |

few studies have been carried out, mainly to characterize the microstructure of dynamically vulcanized TPEs based on different rubber-plastic blend systems.

Although, both looks confusingly similar, the dynamic reaction does not involve the usage of curing agents like sulfur but instead it involves an additional polymer entity which chemically reacts with the free functional groups in the rubber and olefin simultaneously and thereby enhance the miscibility.

In this paper is to follow the morphology changes during the mixing process for a model material for truck tire and polypropylene (PP) blend system (65/35 w/w) with a compatibilizer. SEM examination was carried out on the quickly quenched samples taken from the twin screw extruder along the screw by cooling the experimental set up and also after the onset of the crosslinking of the rubber phase of the samples. The morphology development was studied by using cryogenically fractured etched samples in *p*-xylene. After consideration of the variation of interfacial adhesion between the two phases during the mixing process, a four-stage model is suggested and discussed.

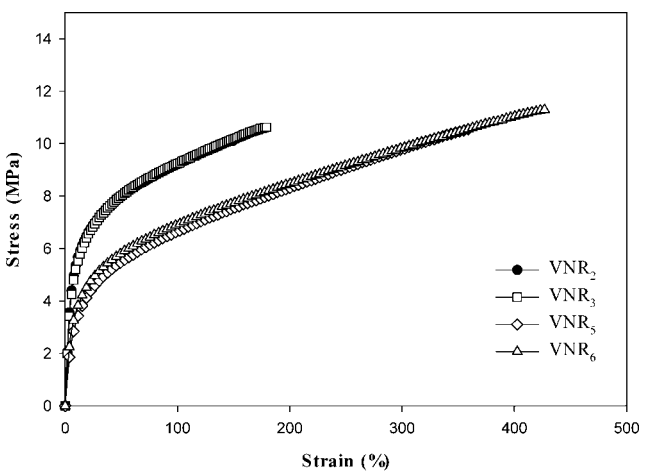


**Figure 4** The tensile properties of model material with isotactic PP and maleic anhydride grafted PP blends prepared by addition of compatibilizers.

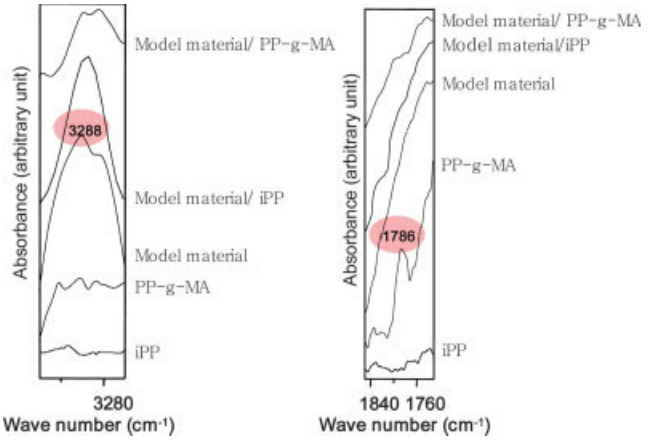


**Figure 5** FTIR ATR spectra of the PP-*g*-MA, model material and PP-*g*-MA/model material blends. [Color figure can be viewed in the online issue, which is available at www.interscience.wiley.com.]

## RESULTS AND DISCUSSION

### Tensile properties of model material/polypropylene blends

Figure 3 shows the tensile properties of the model material with isotactic PP and maleic anhydride grafted PP blends. These model material/isotactic PP blends are simply a physical mixture of two incompatible polymers in which a continuous plastic phase is largely responsible for the tensile properties. Tensile strength of model material/PP-*g*-MA blends are lower than that of model material/isotactic PP blends but elongation at break is higher as can be observed from Table VI. In the case of compounds derived from isotactic PP, the elongation at break decreased because of the incompatibility of the phases in the compound. In the incompatible compounds, the adhesion between the phases is poor, resulting in the tensile properties being dependent on the matrix phase properties. The low values of elongation at break reflect the delamination that occurs during tensile deformation because of poor interfacial adhesion.[14] The tensile property of isotactic PP matrix phase is higher than rubber domain component. To get better properties, the rubber particles need to be sufficiently small and adhering to the matrix by a compatibilizer to the reactive func-

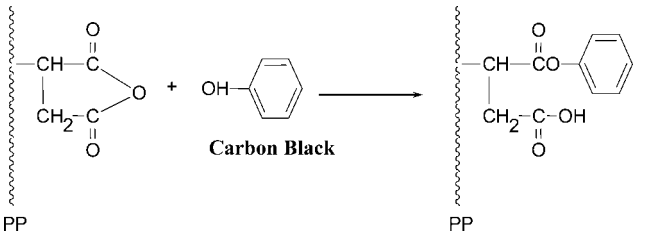


**Figure 6** Chemical reaction between functional groups.

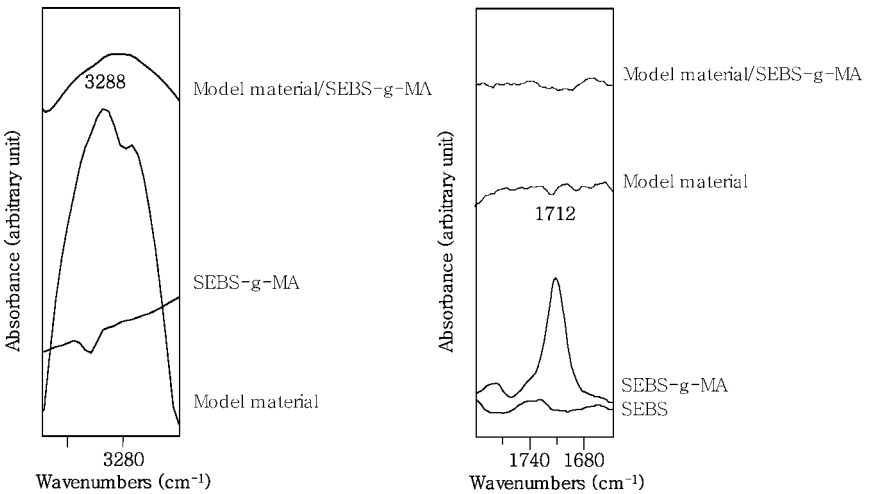


**Figure 7** The FTIR ATR spectra of the SEBS-*g*-MA, model material and model material/SEBS-*g*-MA.

tional group in the polymer for example maleic anhydride on PP-*g*-MA. Therefore, in the case of compounds compatibilized by PP-*g*-MA, a slight increase of the elongation at break of the compound were observed.

This can be explained by the plasticizing effect of the compatibilizers to the phases in the compound resulting in the tensile properties being dependent on both the matrix and domain phase properties. This also shows that the tensile strength increases in the PP-*g*-MA blend with addition of SEBS and more by SEBS-*g*-MA. Thus, one can see that tensile strengths of model material/PP-*g*-MA blends are better than those of model material/isotactic PP blends.

Figure 4 shows that in the case of polar compatibilizers used for model material/PP compounds, the functional polymer SEBS-*g*-MA gave the best tensile properties of all the model material/PP compounds both for isotactic PP and PP-*g*-MA. It has also been shown that PP has good compatibility with the EB (ethylene-*co*-butylene) block copolymer because of the repulsion effect[15] of ethylene and butylene segments that might contribute to the improvement of the miscibility of PP with model material. Mainly, the reactive functional group Viz. MA (maleic anhydride) is in reaction with carbon black on the model material while the EB mid block of the SEBS copolymer has also good compatibility with PP, thereby the model material, PP-*g*-MA and compatibilizer (SEBS or SEBS-*g*-MA) compound forms a stable three network system. Similarly, Rajalingam and Baker[16] had observed that EAA (ethylene-acrylic acid) acts as an interfacial coupling agent for carbon black, metal oxide, or other polar species, on the GRT surface.

### Chemical interaction between the model material/polypropylene blends

The changes in the tensile properties are the result of changed structure, indicating the strong effect of chemical interactions between the polymers. Bikiaris et al.[17] has found that MA from PP-*g*-MA reacted with hydroxyl group in silica and confirmed it by FT-IR spectra. Likewise, Qiu et al. found that MA grafted polypropylene reacted with —OH group in cellulose and confirmed it by FT-IR spectra.[18] Figure 5 shows the FTIR ATR spectra of the isotactic PP, PP-*g*-MA, model material and model material/PP. The peak at 3288 $cm^{-1}$ corresponds to the —OH stretching vibration of hydroxyl group present in

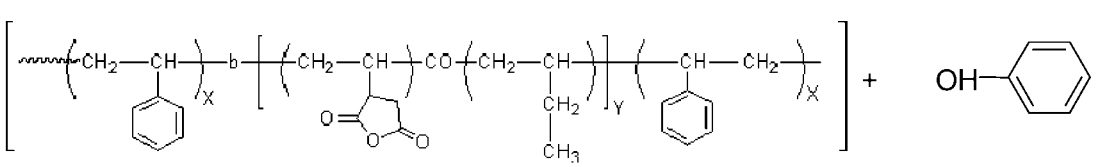


Maleic anhydride grafted Polystyrene-b-poly[ethylene-co-(but-1-ene)]-b-Polystyrene Triblock Copolymer

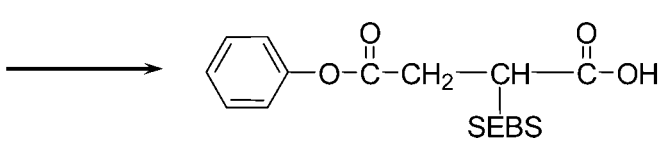


**Figure 8** Mechanism of interaction.

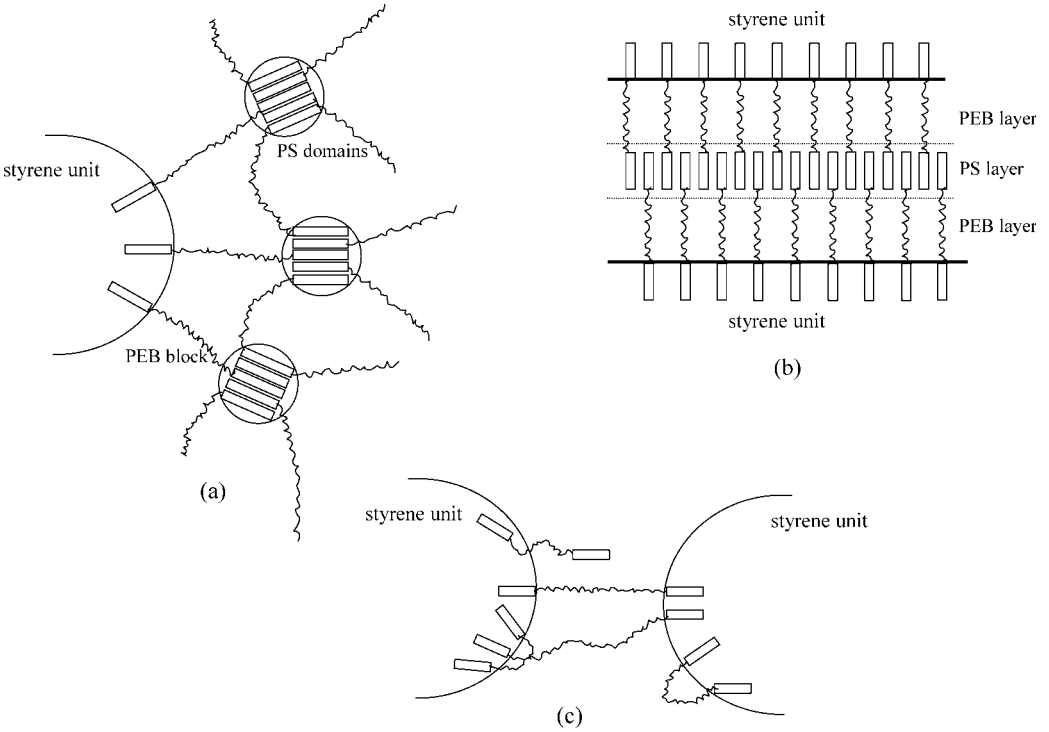


**Figure 9** Proposed SEBS triblock copolymer conformations in the dispersed SBR/SEBS aggregates: (a) Formation of spherical PS mirodomains, (b) formation of lamellar microdomains, and (c) disordered interparticle region [48].

the model material Donnet et al.[19] and Pena et al.[20] have found that —OH groups are also present on the surface of carbon black. This peak absorbance value decreases in the model material/PP-*g*-MA indicating the interaction between the phenolic —OH group in the carbon black with maleic anhydride. It is possible that chemical reaction proceeded between maleic anhydride from PP-*g*-MA and hydroxyl groups in the carbon black[21] in model material. This is further supported by the disappearance of the peak at 1786 $cm^{-1}$ that corresponds to the >C=O stretching vibrations of maleic anhydride group in the PP-*g*-MA backbone. Therefore, the possible mechanism of interaction can be visualized as shown in Figure 6.

### Chemical interaction between the model material and compatibilizers

It is also possible that chemical reaction proceeded between maleic anhydride from SEBS-*g*-MA which was used as a compatibilizer and hydroxyl groups in the carbon black in model material, although it is not visible from the FTIR ATR spectra clearly. Tselios et al.[22] found that MA grafted polystyrene reacted with hydroxyl group in poly(ethylene-*co*-vinyl alcohol) and confirmed it by FT-IR spectra. Figure 7 shows the FTIR ATR spectra of the SEBS-*g*-MA, model material and model material/SEBS-*g*-MA. The peak at 3288 $cm^{-1}$ corresponds to the —OH stretching vibration of hydroxyl group present in the model material. The peak absorbance value decreases in the model material/SEBS-*g*-MA indicating the interaction between the phenolic —OH group with maleic anhydride as suggested in the mechanism. Therefore, the possible mechanism of interaction can be visualized as shown in Figure 8.

This is further supported by the disappearance of the peak at 1712 $cm^{-1}$ that corresponds to the —C=O stretching vibrations of maleic anhydride group in the SEBS backbone. This explanation is in

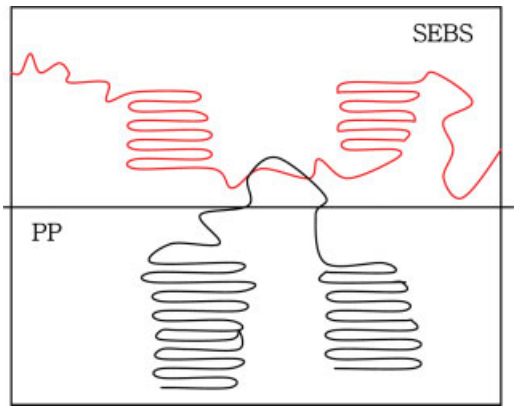


**Figure 10** The interaction on the interface between the matrix and the compatibilizers [49]. [Color figure can be viewed in the online issue, which is available at www.interscience.wiley.com.]

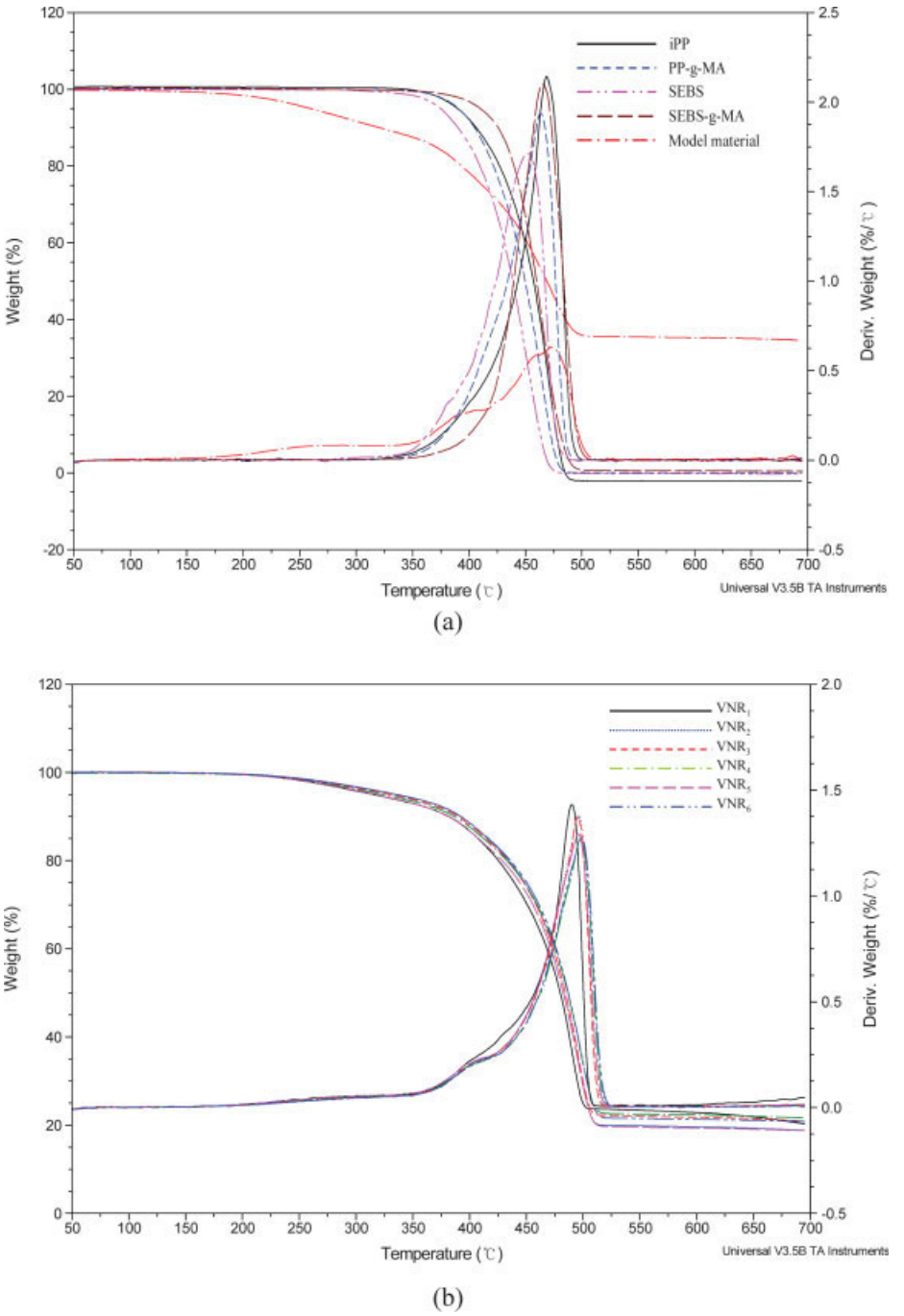


**Figure 11** TGA cuvers for (a) base materials and (b) model material/PP TPVs. [Color figure can be viewed in the online issue, which is available at www.interscience.wiley.com.]

accordance with the work of Tjong and Xu.[23] The possible mechanism of interaction has been shown in the Figure 9.

For triblock SEBS, bilateral PS end-blocks form microdomains and the EB mid-block connect between PS microdomains like a loop or a bridge in the micro phase-separated structure. Here, the PS microdomains play an important role as cross-linking points. Therefore, triblock SEBS has much stronger tensile properties than diblock SEB. Moreover, the cross-linking effect of PS microdomains strongly affects the reinforcement of interfacial adhesion. The entanglement between PP chain and EB chain, i.e. PP chains hook through EB chains like a loop or bridge, which we call ''hooking effect'', will reinforce the interfacial connection at the PP/triblock SEBS interface. The possible mechanism of interaction has been shown in the Figure 10.

**TABLE VII**
**TGA of Base Materials and Model Material/PP TPVs**

| Sample | $T_{5\%}$ mass loss (°C) | $T_{10\%}$ mass loss (°C) | Temperature for maximum rate of degradation (°C) |
|---|---|---|---|
| iPP | 387 | 405 | 469 |
| PP-*g*-MA | 391 | 405 | 463 |
| SEBS | 375 | 390 | 452 |
| SEBS-*g*-MA | 410 | 426 | 465 |
| Model material | 259 | 321 | 474 |
| $VNR_1$ | 315 | 382 | 490 |
| $VNR_2$ | 316 | 381 | 496 |
| $VNR_3$ | 330 | 390 | 495 |
| $VNR_4$ | 323 | 386 | 498 |
| $VNR_5$ | 336 | 393 | 496 |
| $VNR_6$ | 336 | 392 | 498 |

## Thermogravimetric analysis

Model material blends with isotactic PP and PP-*g*-MA were subjected to thermal analysis in nitrogen ($N_2$). The respective TGA curves are shown in Figure 11 and reported in Table VII.

The TGA curves obtained at a heating rate of 20°C/min of the binary and ternary blends with various compositions are shown in Figure 11 with the corresponding parameters being given in Table VII. The initial decomposition temperature and overall degradation values of all the model material/isotatic PP changed very little when compared to their PP-*g*-MA counterparts. In the model material/PP-*g*-MA compounds the 5% and 10% mass loss temperature is higher than the model material/isotactic PP compounds. In this study, two kinds of resins and compatibilizers, polar and nonpolar materials, were employed. The polar compatibilizer considered are SEBS-*g*-MA, while the nonpolar is the SEBS. In the case of polar compatibilizer used for model material/PP compound, the functional polymer as SEBS-*g*-MA gave the best thermal stability of model material/PP compounds both for isotactic PP and PP-*g*-MA, particularly when 10 phr of SEBS-*g*-MA were used. The higher thermal stability of the compound compatibilized with SEBS ($VNR_5$) or SEBS-*g*-MA ($VNR_6$) than the compound model material/PP-*g*-MA ($VNR_4$) can be explained by the fact that the EB midblock of the SEBS copolymer gave better compatibility with PP. This explanation is in accordance with the work of Setz et al.[24] It had been shown that PP has good compatibility with the EB block copolymer because of the repulsion effect of ethane and but-1-ene segments that might contribute to the improvement of the miscibility of PP with model material as mentioned earlier.[24] The thermal stability of these material ($VNR_5$, $VNR_6$) is dependent on the PP thermal stability. All TPV samples based on model material started to lose mass at about 220°C.

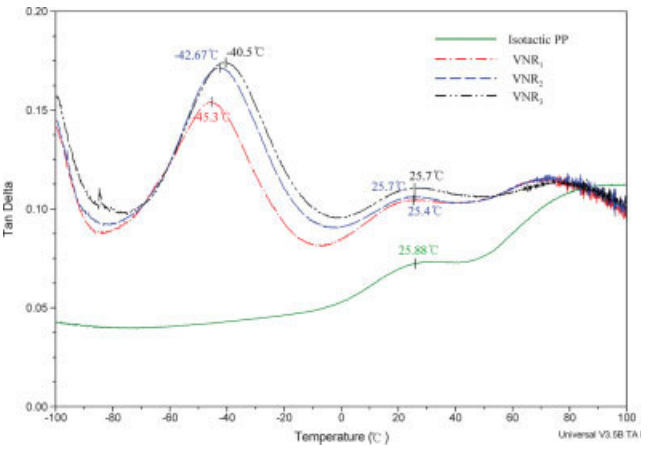


**Figure 13** The effect of compatibilizers in model material/isotactic PP blends on tan δ peaks. [Color figure can be viewed in the online issue, which is available at www.interscience.wiley.com.]

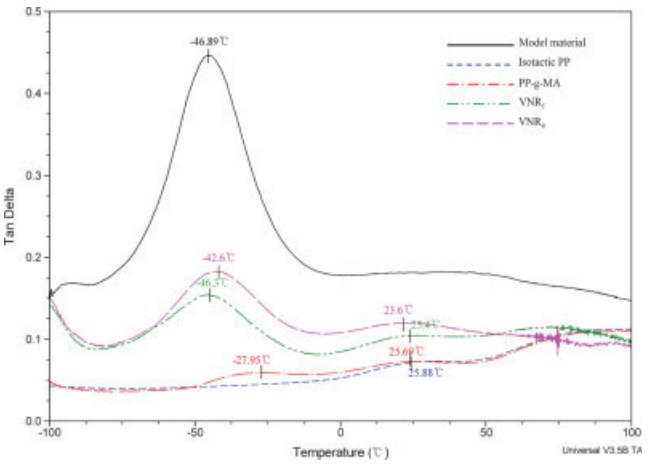


**Figure 12** The tan δ peaks are plotted for model material blends with different olefins. [Color figure can be viewed in the online issue, which is available at www.interscience.wiley.com.]

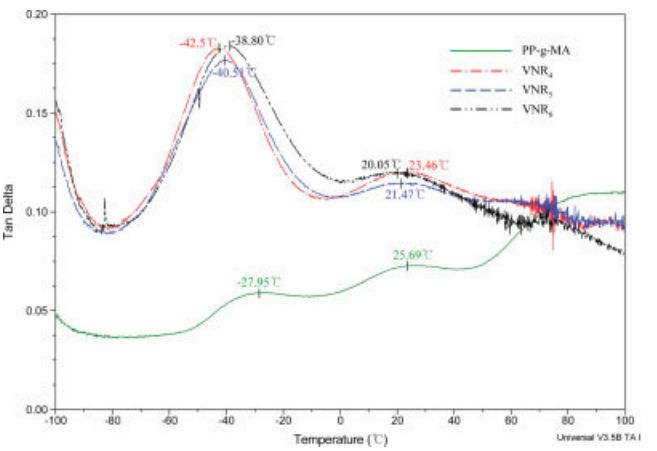


**Figure 14** The effect of compatibilizers in model material/PP-*g*-MA blends on tan δ peaks. [Color figure can be viewed in the online issue, which is available at www.interscience.wiley.com.]

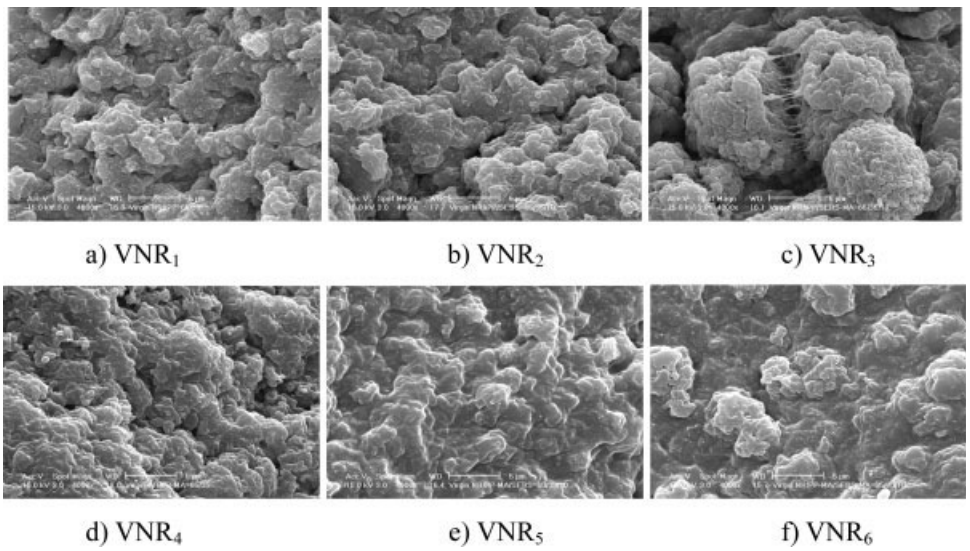


**Figure 15** The morphological changes of the model material blends with different olefins with different compatibilizers.

### Dynamic mechanical properties

Dynamic mechanical investigation is an important tool used to predict the miscibility of polymeric system by researchers. The dynamical mechanical properties such as storage modulus (E′), loss modulus (E″) and damping factor (tan δ) are indicative of the miscibility of the polymer blend by the shift in the position and the breadth of the transition peaks. Generally, for incompatible blends, the tan δ versus temperature curve shows the presence of two tan δ or damping peaks corresponding to the glass transition temperatures of the two individual polymers. For a highly compatible blend, the curve shows only a single peak in between the transition temperatures of the component polymers, whereas broadening of the transition occurs in the case of a partially compatible system. In the case of compatible and partially compatible blends, the $T_g$'s are shifted to higher or lower temperatures as a function of composition. Since tan δ is commonly used for such studies, Figure 12 shows the plot for model material blends with different olefins and the corresponding neat olefins from −100°C and 30°C.

Two peaks are present in all blends due to phase separation, the lower temperature peak (−45°C) is for soft elastomer segment and the higher temperature peak (+25°C) is for hard thermoplastic segment. The $T_g$ of the soft portion increases in the compound when PP-*g*-MA was blended with model material, however, the $T_g$ of hard portion decreases. In the case of isotactic PP, only one peak was observed by Grein et al.[25] which was also observed here and in this case at 25.9°C. But, an extra peak was observed for neat PP-*g*-MA Viz. the dominant relaxation appearing at around −28°C is due to the glass-rubber relaxation of amorphous portions of the PP-*g*-MA solid. In the case of blend involving PP-*g*-MA, the lower temperature peak on PP-*g*-MA disappeared when added with the model material because of the MA (maleic anhydride) group has been consumed during the reaction with polar group in the model material. As a result, the $T_g$ of the soft portion increase and hard portion decrease with respect to temperature in the model material/PP-*g*-MA blend. The effect of compatibilizers in model material/isotactic PP blends is demonstrated in Figure 13, where the $T_g$ of soft segment shifted toward higher temperature, but the $T_g$ of the hard segment remains the same. With the addition of SEBS-*g*-MA as compatibilizer, the $T_g$ of soft segment is higher than the SEBS added blend. Particularly, for model material/isotactic PP compounds compatibilized with 10 phr SEBS and 10 phr SEBS-*g*-MA, the soft portion was significantly increased up to −42.67°C for SEBS and −40.5°C for SEBS-*g*-MA from −46.3°C. This is due to sufficient adhesion with the dispersed phase. However, when the PP-*g*-MA was blended with model material with these same compatibilizers, these two peaks changed (see Fig. 14). The $T_g$ of soft

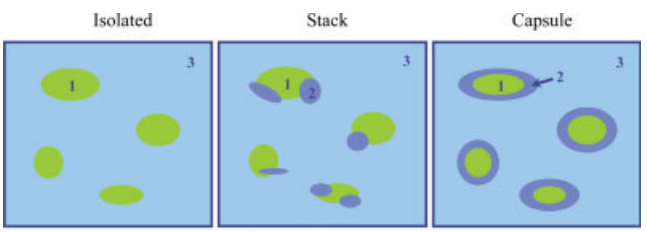


**Figure 16** Schematic description of phase formation in ternary polymer blends. [Color figure can be viewed in the online issue, which is available at www.interscience.wiley.com.]

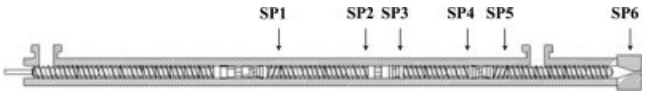


**Figure 17** Sampling points for extrusion.

segment tends to increase, and the $T_g$ of hard segment tends to decrease with the addition of compatibilizers. The compatibilizer seems to act as a plasticizer to PP-g-MA. It is further observed that when SEBS-g-MA as compatibilizer was used in model material/PP-g-MA, the $T_g$ of soft segment is higher whereas, the $T_g$ of hard segment decreases compared to model material/isotactic PP blends with the same compatibilizer. This is due to sufficient adhesion between the matrix phase and the dispersed phase.

### Morphological properties

The morphological changes of the model material blends with different olefins and their blends with different compatibilizers are shown in Figure 15(a–f).

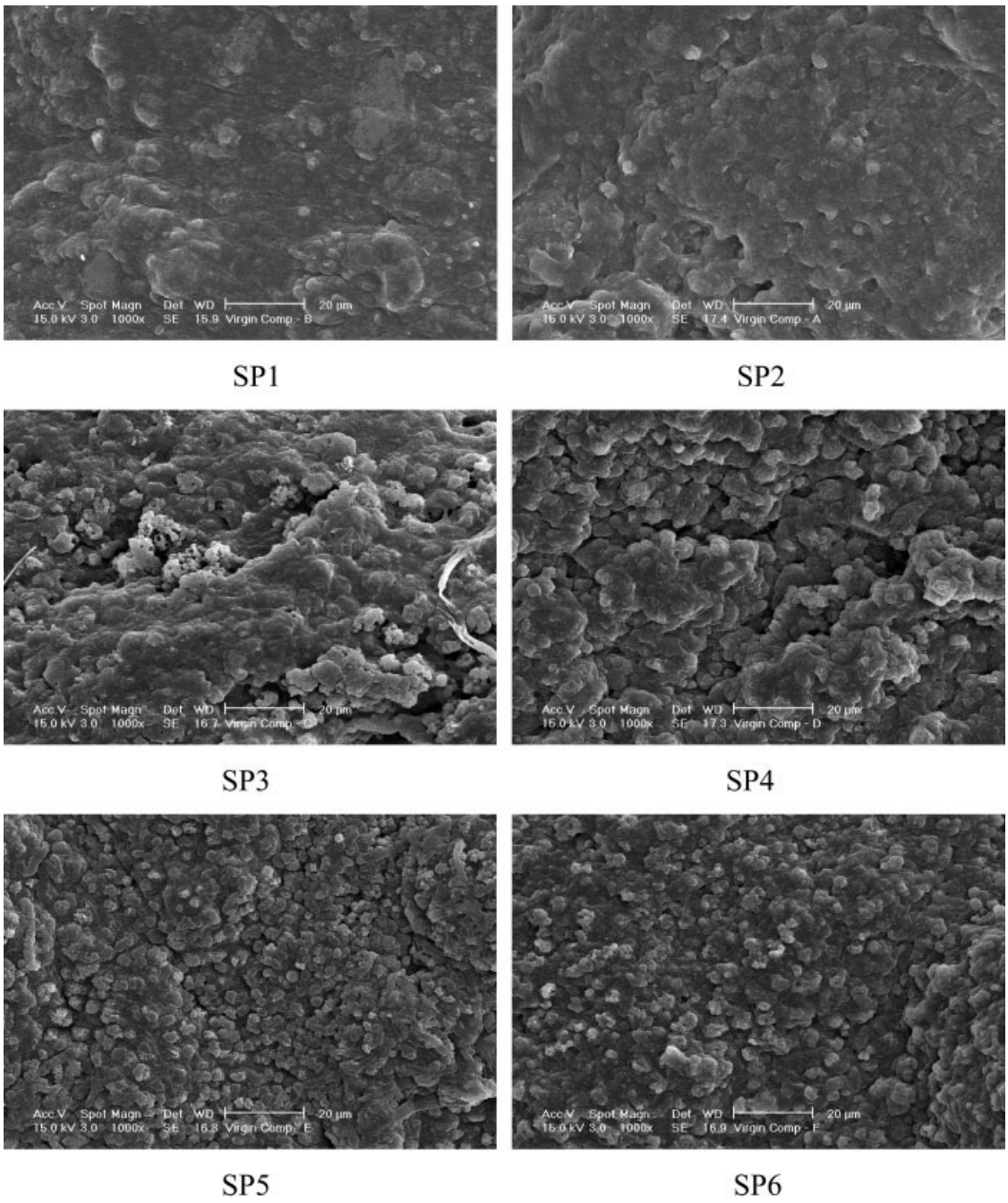


**Figure 18** SEM photographs of model material/PP-*g*-MA blends sampled at different positions along the length of the extruder.

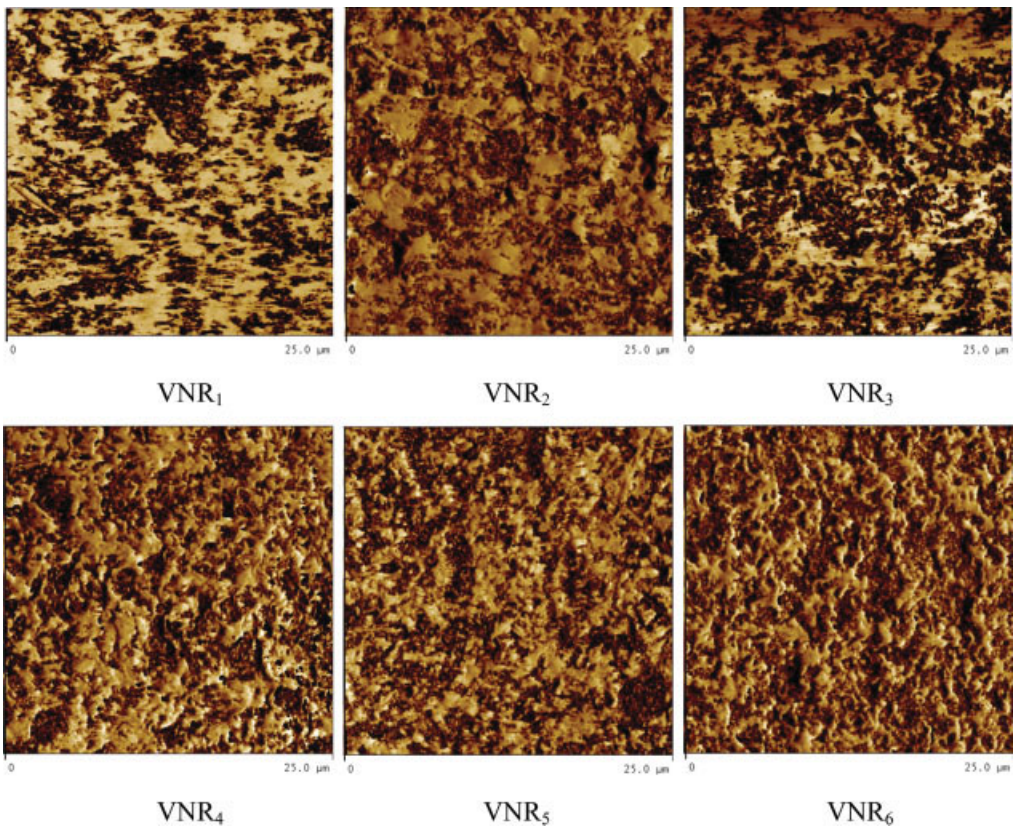


**Figure 19** The effect of compatibilizer on the interface morphology in the AFM (scale 25 μm). [Color figure can be viewed in the online issue, which is available at www.interscience.wiley.com.]

The two olefins Viz. isotactic PP & PP-*g*-MA exhibited different surface morphologies, as well as those in different compatibilizers in their blend systems; nevertheless it contains two dispersed phases due to the thermodynamic incompatibility of the constituents. The surface morphology of model material blends with isotactic PP series has elongated dispersed phase particles of rubber [see Fig. 15(a–c)], while those blends with PP-*g*-MA exhibited a smooth surface with small dispersed phases in a continuous matrix [Fig. 15(d–f)]. With the addition of SEBS compatibilizer as shown in Figure 15(b,c), the elongated dispersed phase becomes more spherical in shape, and those blends with SEBS-*g*-MA [Fig. 15(e,f)], the surface becomes smoother and the dispersed particles are more visible in a continuous phase of matrix. However, when SEBS-*g*-MA was used in the model material/isotactic PP blends, the dispersed phases developed into larger particles as shown in Fig. 15(b,c). The effect of SEBS-*g*-MA in model material/PP-*g*-MA blends is different. The continuous hard phase and the dispersed phase of soft segment are clearly visible with smoother surfaces. From the above results, a schematic description of the phase formation in ternary blends was proposed. This is shown in Figure 16.

In this study, model material/PP-*g*-MA is blended in the extruder and once the extrusion process is continuously operating smoothly, suddenly stopped and samples were taken during stationary extruder conditions by opening the individual sample plates. These samples were immediately cooled down in liquid nitrogen in order to avoid morphology changes. With this quick sampling technique it was possible to take the sample out from the extruder within 5–10 s and frozen, thus allowing coalescence processes to be ignored. Figure 17 shows the sampling points in the twin screw extruder.

For the quantitative morphology analysis and in order to achieve a good contrast, it was necessary to dissolve the PP matrix phase. For this reason, the samples were boiled in *p*-xylene for 30 min. The etched samples were then prepared for the investigations with the SEM. The SEM photographs of blend are shown in Figure 18 from different sampling points. In this figure, as the feed moves from the hopper to the die, the initial PP matrix/rubber domain is changed into rubber matrix/PP-*g*-MA domain along the screw position. It can also be observed from the SEM micrographs that the model material particles are finely dispersed as very small size particle in the PP-*g*-MA matrix (Fig. 15).

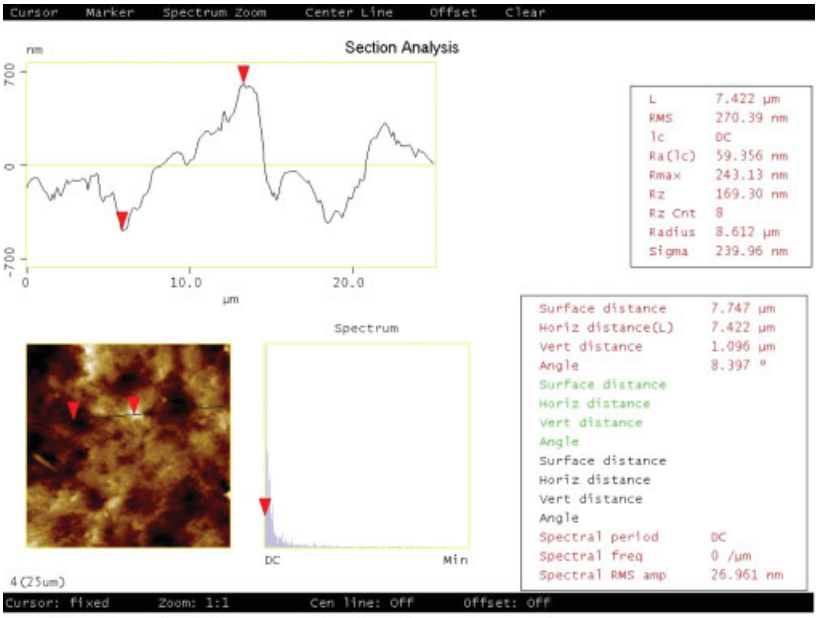


**(a)**

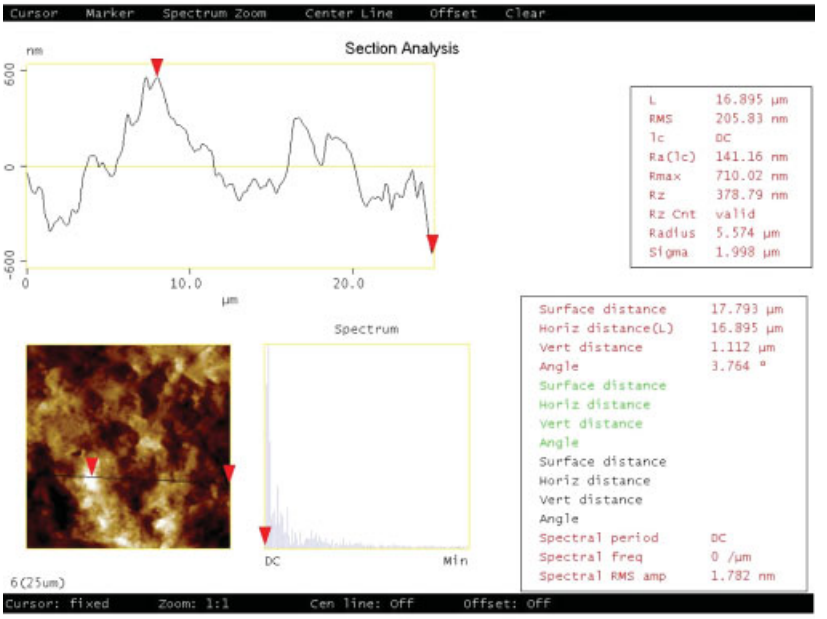


**(b)**

**Figure 20** The AFM section analysis of samples (a) $VNR_1$ (b) $VNR_3$ (c) $VNR_4$ and (d) $VNR_6$. [Color figure can be viewed in the online issue, which is available at www.interscience.wiley.com.]

AFM (Atomic Force Microscope) was also used to evaluate the effect of compatibilizer on the interface morphology. Figure 19 (scale 25°C) shows, the AFM phase image of 65/35 model material/iPP blends ($VNR_1$), PP-*g*-MA ($VNR_4$), isotactic PP with SEBS and SEBS-*g*-MA ($VNR_2$, $VNR_3$), PP-*g*-MA with SEBS and SEBS-*g*-MA ($VNR_5$, $VNR_6$), respectively. The dynamic reaction undergone model material (bright phase) and dispersed compatibilizers (dark-bright phase) is seen to be dispersed in the dark PP matrix.

In the PP-*g*-MA blend, the domain size of the model material dispersed phase in compatibilized blends is much smaller than that of its isotactic PP blend counterpart. It is believed that the retardation of phase growth in the PP-*g*-MA blends take place and the morphology of the PP-*g*-MA blends with compatibilizer is more stable than that of the isotactic PP blend due to the reaction between model material and PP during extrusion by reactive functional group (maleic anhydride) in PP-*g*-MA. The func-

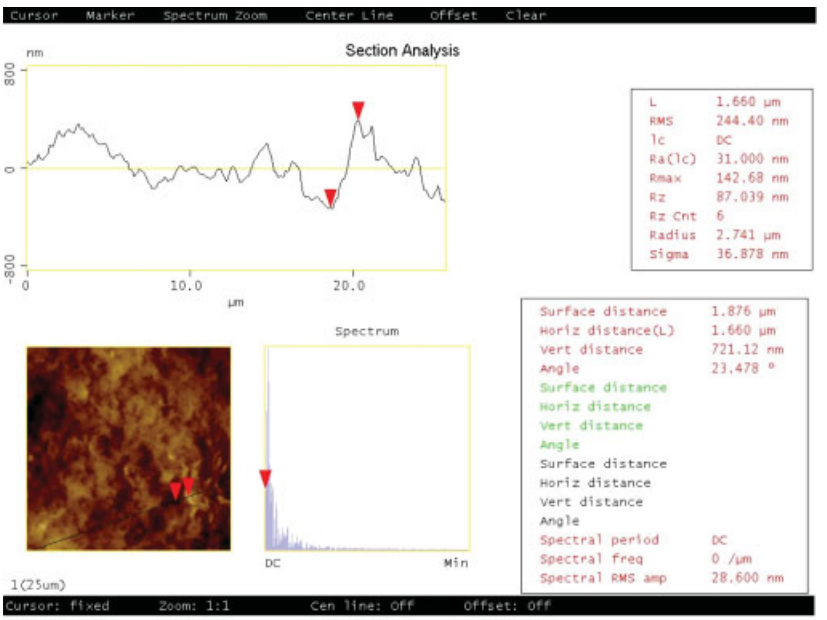


**(c)**

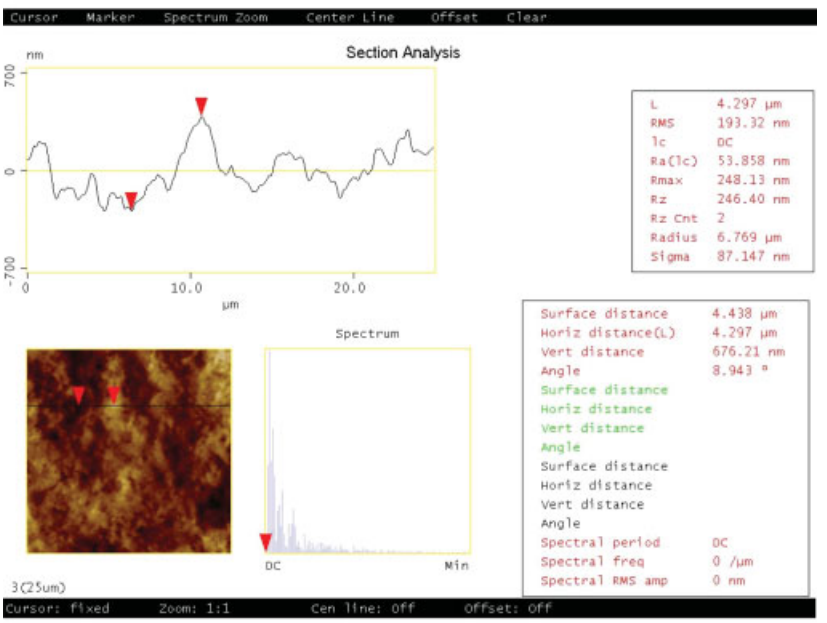


**(d)**

**Figure 20** (*Continued from the previous page*)

tional group and compatibilizers leads to enhanced chemical interaction at the interface and improved adhesion between the two polymers.

Figure 20 shows the three-dimensional AFM surface profile and section analysis of the AFM images. A three-dimensional AFM surface profile and section analysis represent the interfacial topology between model material and PP phase. There are sharp steps developed at the interface between the model material and the isotactic PP. The surface topology at each side of the step is relatively flat. These sharp steps as well as the presence of delamination regions indicate the poor adhesion between model material and PP phase. Model material and PP have different thermal expansion coefficients and expand differently after the cryo-microtoming procedure. Because of the weak adhesion at the interface between the model material and PP, sharp steps have been developed upon reactivity between model material, PP and compatibilizer. In the case of $VNR_1$ and $VNR_3$, the height of the steps is about 1.1 nm. In contrast to the isotactic PP blends, the three-dimensional surface

profile does not reveal sharp steps at the interface in the PP-*g*-MA blends. The sectional analysis illustrates a smooth step with the height about 721 nm in the blend with PP-*g*-MA and 676 nm in the PP-*g*-MA blend with compatibilizer, which are almost one order of magnitude smaller compared to the isotactic PP blend. Furthermore, AFM three-dimensional images reveal some interfacial roughening at the interface between the model material and PP-*g*-MA blends. This indicates much better adhesion at the interface in the model material/PP-*g*-MA blends which correlates well with their higher tensile properties.

The development of the interfacial roughening as well as improvement of the interfacial adhesion in an immiscible PET/PS blend due to the formation of copolymer upon addition of a reactive compatibilizer was reported by Maa et al.[26] and Lyu et al.[27] have also reported interfacial reaction between two immiscible polymers due to the creation of *in-situ* copolymer. Thus, the AFM observation allowed us to visualize the interfacial topology changes due to the formation of *in-situ* model material/PP copolymer by means of functional group in model material and polar compatibilizer. The formation of the copolymer at the interface creates the interfacial roughness and eventually glues the two phase together, which prevents the step formation.

## CONCLUSIONS

The blends of a truck tire model rubber material and PP thermoplastic are simply a physical mixture of two incompatible polymers in which a continuous plastic phase is largely responsible for the tensile properties. The large particle size and the poor adhesion are believed to be liable for the poor properties. Also, the tensile properties of truck tire model material with isotactic polypropylene are found to be lower than that of its PP-*g*-MA counterpart because of reaction occurring in PP-*g*-MA blend. The addition of compatibilizers such as SEBS and SEBS-*g*-MA induces an increase in the tensile properties for both types of polyolefins but always higher for the PP-*g*-MA based blends. The occurrence of this reaction is confirmed by the FT-IR data which indicates the interaction between the phenolic —OH group in model material with maleic anhydride group of PP-*g*-MA. A reaction mechanism for the dynamic reaction has been proposed and it is later confirmed by thermal analysis and dynamic mechanical studies. In the DMA study, two peaks are present in all the blends due to phase separation, the lower temperature peak is for elastomer segment and the higher temperature peak is for thermoplastic segment. The results of this study showed that when compatibilizer was added in model material/PP-*g*-MA blends, the $T_g$ of soft segment is shifter to higher, whereas, the $T_g$ of hard segment is shifted to lower temperatures compared to model material/isotactic PP blends of the same compatibilizer. The surface morphology of model material/isotactic PP blends shows elongated dispersed phase of rubber particles while those blends with PP-*g*-MA exhibits a smooth surface with relatively small dispersed phases in a continuous matrix. However, with the addition of SEBS-*g*-MA compatibilizer, the elongated phase of model material/isotactic PP blends becomes spherical in shape and those with PP-*g*-MA the surface becomes smoother and the dispersed particles are more clearly visible. In this chapter, it is also clearly showed that morphological changes occur in the blends in the presence of compatibilizers during the melt blending along the length of the twin screw extruder. The blends of model material and PP-*g*-MA with compatibilizers have better adhesion compared to those of isotactic PP blends counterparts as revealed by the AFM results. Better adhesion between the two polymers with compatibilizer is further shown in the three-dimensional AFM profile, which illustrated smooth and smaller steps than isotactic PP blends. It also does not reveal any sharp steps at the interface.

## References


1. Nevatia, P.; Banerjee, T. S.; Dutta, B.; Jha, A.; Naskar, A. K.; Bhowmick, A. K. J Appl Polym Sci 2002, 83, 2035.
2. Shahidi, N.; Teymour, F.; Arastoopour, H. Macromolecular Symposia 2004, 206, 471.
3. Liu, H.; Mead, J. L.; Stacer, R. G. Rubber Chem Technol 2002, 75(1), 49.
4. Jacob, C.; De, P. P.; Bhowmick, A. K.; De, S. K. J Appl Polym Sci 2001, 82, 3293.
5. Jacob, C.; De, P. P.; Bhowmick, A. K.; De, S. K. J Appl Polym Sci 2001, 82, 3304.
6. Coran, Y.; Patel, R. P. In Thermoplastic Elastomers Based on Dynamically Vulcanized Elastomer-Thermoplastic Blends in Thermoplastic Elastomers, 2nd ed.; Holden, G., Legge, N. R., Quirk, R., Schroeder, H. E., Eds.; Hanser/Gardner Publications: Cincinnati, USA, 1996.
7. David, S.; Jeff, A. Rubber World 1999, 219, 22.
8. Montoya, M.; Tomba, J. P.; Carella, J. M.; Gobernado-Mitre, M. I. Eur Polym J 2004, 40, 2757.
9. Jurkowska, B.; Jurkowski, B. J Appl Polym Sci 2003, 90, 2583.
10. Goharpey, F.; Katbab, A. A.; Nazockdast, H. J Appl Polym Sci 2001, 81, 2531.
11. Fisher, W. K. U.S. Pat. 375,643.
12. Coettler, L. A.; Richwine, J. R.; Wille, F. J. Rubber Chem Technol 1982, 55, 1448.
13. Moffett, A. J.; Dekkers, M. E. J. J Polym Eng Sci 1992, 32, 1.
14. Montiel, A. G.; Keskkula, H.; Paul, D. R. Polymer 1995, 36, 4605.
15. Setz, S.; Stricker, F.; Kressler, J.; Duschek, T.; Mulhaupt, R. J Appl Polym Sci 1996, 59, 1117.
16. Rajalingam, P.; Baker, W. E. Rubber Chem Technol 1992, 65, 908.

17. Bikiaris, D. N.; Vassilion, A.; Pavlidon, E.; Karayannidis, G. P. Eur Polym J 2005, 41, 1965.
18. Qiu, W.; Zhang, F.; Endo, T.; Hirotsu, T. Polym Compos 2005, 26, 448.
19. Donnet, J. B.; Bansal, R. C.; Wang, M. In Carbon Black; Donnet, J. B., Ed.; Marcel Dekker: New York, 1993.
20. Pena, J. M.; Allen, N. S.; Liauw, C. M.; Edge, M.; Valange, B. J Vinyl Additive Technol 2000, 6, 62.
21. Roychoudhury, A.; De, P. P. J Appl Polym Sci 1995, 55, 9.
22. Tselios, C.; Bikiaris, D.; Prinos, J.; Panayiotou, C. J Appl Polym Sci 1997, 64, 983.
23. Tjong, S. C.; Xu, S. A. J Appl Polym Sci 2004, 94, 1539.
24. Setz, S.; Stricker, F.; Kressler, J.; Duschek, T.; Mulhaupt, R. J Appl Polym Sci 1996, 59, 1117.
25. Grein, C.; Bernreitner, K.; Gahleitner, M. J Appl Polym Sci 2004, 93, 1854.
26. Maa, C. T.; Chang, F. C. J Appl Polym Sci 1993, 49, 913.
27. Lyu, S. P.; Bates, F. S.; Macosko, C. W. AlChE 2002, 48, 7.